Circulation control on a rounded trailing-edge wind turbine airfoil using plasma actuators

S. Baleriola, Annie Leroy, S. Loyer, Philippe Devinant, S. Aubrun

Circulation control on a rounded trailing-edge wind turbine airfoil using plasma actuators

Circulation control on a rounded trailing-edge wind turbine airfoil using plasma actuators

S. Baleriola, A. Leroy, S. Loyer, P. Devinant, S. Aubrun
Université d'Orléans, INSA CVL, PRISME, EA 4229, F-45072, Orléans, France
E-mail: sophie.baleriola@univ-orleans.fr

Abstract.
This experimental study focuses on the implementation via plasma actuators of a circulation control strategy on a wind turbine aerofoil with a rounded trailing-edge with the objective of reducing the aerodynamic load fluctuations on blades. Three sets of multi-DBD (Dielectric Barrier Discharge) actuators with different positions around the trailing-edge are studied. These actuators create a tangential jet that adheres to the blade model wall and diffuses along it. According to the jet direction, lift is increased or decreased. Load and pressure measurements as well as Particle Image Velocimetry (PIV) show respectively the actuation effectiveness in terms of load modification and flow topology alteration.

1. Introduction and work objectives

Wind energy is one of the most promising renewable energies for the years to come. Its world-wide rate of activity yearly increases of 20%. However, the rotor's operating life can still be improved in order to allow an optimal energy production for periods longer than 20 years. Due to the atmospheric boundary layer, the incoming flow is highly inhomogeneous and unsteady and it induces, via strong wind gusts, significant load fluctuations on wind turbine blades. This project is part of the French national project SMARTEOLE that aims at optimizing the wind energy efficiency by developing innovative control concepts with the intention of reducing load fluctuations on blades. The cost of energy will be therefore reduced by extending the lifetime of the wind turbine rotors. The SMARTEOLE project deals with different control strategies at different scales from blade chord scale to wind farm scale. The present study deals with the actuation at the blade scale and focuses on the plasma modification of the local trailing-edge flow.

To reduce the aerodynamic load fluctuations, a circulation control strategy is considered. The displacement of the streamline separation point and of the rear stagnation point is allowed by a rounded trailing-edge aerofoil. This flow modification at the trailing-edge allows the monitoring of the circulation and consequently a regulation of the lift force that can be either increased or decreased. Figure 1 shows the principle of this circulation control actuation in response to a sudden gust modifying the incoming flow speed and the angle of attack. The aim of the flow control is to maintain a constant lift force whatever the incoming wind conditions are. The working range of angles of attack is located along the linear part of the lift curve where the flow is attached to the airfoil.

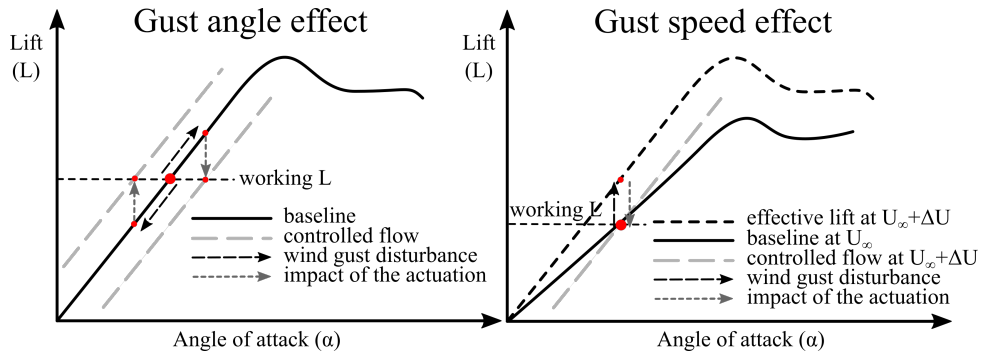

Figure 1. Principle of circulation control in response to a sudden gust modifying the incoming flow speed and angle of attack

A large number of experimental and numerical studies investigated circulation control on aerofoils ([1], [2]). Most of them deal with fluidic tangential jets that permit circulation control and the use of the Coanda effect over a curved surface allowing the flow to adhere the curved wall. One common application is the actuation at the trailing-edge of an airplane wing in order to replace the mechanical moving parts such as control surfaces or flaps. Nowadays, the circulation control technique is mainly investigated with wind turbine applications in view [3].

Dielectric Barrier Discharge (DBD) plasma actuators are interesting devices regarding their ability to modify the flows in a completely electrical way. These actuators create a tangential ionic wind near the wall that permits flow manipulation. One can find in [4] a review of the electrical and mechanical characteristics of DBD plasma actuators applied to airflow control. In order to take advantage of the Coanda effect along curved surfaces, it is usually necessary for conventional fluidic jets to be characterized by a high momentum coefficient as exposed in [1]. Although the flow mass rate of the induced tangential jet generated by DBD actuators remains low compared to fluidic jets, the induced jet is supposed to adhere to curved surfaces because the ionic wind is generated by momentum transfer occurring very close to the electrodes following the electric field distribution.

In the field of applied aerodynamics, active flow control with plasma actuators is implemented to either perform a boundary layer separation control or a circulation control. Separation control consist in an action at the leading-edge of the airfoil that delays stall to higher angles of attack such as leading-edge slats devices, for example. On the other hand, circulation control results of an action at the trailing-edge of an airfoil that shifts the lift curve towards higher (or lower) lift forces as it can be done with trailing-edge flaps. Compared to other flow control strategies, plasma actuators have the benefit of being small, light and do not require mobile parts. Furthermore, as the system is purely electrical and not mechanical, their time response is smaller than the millisecond, which is particularly interesting for active flow control applications.
Regarding separation control with DBD plasma actuators, Walker and Segawa [5] worked with a NACA0024 aifoil in a 2D configuration at a Reynolds number of 130000. Their work highlighted the importance of the actuator location along the chord of the airfoil: the actuation was more efficient when the DBD actuator was implemented close to the separation point when working between the leading-edge and 25% of the chord length. Numerical simulations of separation control with DBD actuators in a 2D set-up proved also promising results as shown in [6]. Greenblatt et al. [7] implemented plasma actuators at the leading-edge of a vertical axis wind turbine up to $Re = 210000$ in order to monitor the boundary layer separation and avoid the dynamic blade stall that induces load fluctuations on blades. By the effect of the actuation, the turbine power

was improved up to 38%. Jukes implemented DBD vortex generators along the blade span on a horizontal axis wind turbine [8]. Rotating stall control was demonstrated and therefore the lift force on blades could be increased as well as the turbine power output.
A few studies focus on circulation control around wind turbine blades using plasma actuators. Zhang et al. [9] carried out RANS numerical simulations on an elliptical airfoil and obtained a lift coefficient gain ΔC_l of 0.8 for a Reynolds number (Re) of 684000. Kotsonis et al. performed an experimental study with a symmetrical NACA airfoil [10] and proved a ΔC_l of 0.1 for a Re of 140000. The importance of the actuator position around the trailing-edge roundness as a function of the angle of attack is also highlighted by the authors. Leroy et al. [11] carried out a preliminary study with the same airfoil that is used in this project and have shown a ΔC_l of 0.1 ($Re = 200000$) for thin dielectric DBD plasma actuators. In the present work, a thick dielectric material is used in the aim of working with a large range of voltage applied to the actuator. Hence, the lift increase can be defined as a function of the input voltage and it could be determined if the applied voltage can be a suitable control command parameter. In addition to a usual and essential lift increase, a lift decrease will be also be carried out in this project.

The objective of this experimental work is to demonstrate the open-loop feasibility of an active circulation control with plasma actuators. Hence, it will only be explained in this paper how the implemented flow control is able to modify the aerodynamic loads such as the translation of the lift curve towards higher or lower lift coefficients or the modification of the pressure distribution with the actuation. The modification of the wake topology with the control will also be discussed.
The first part of the paper summarizes the experimental means and facilities used in this study as well as the specifications of the implemented plasma actuators. The second part describes the plasma jet topology under quiescent air conditions via a flowfield characterization study using PIV. The effects of the actuation on the aerodynamic loads and on the wake topology are described on the last part of the paper.

2. Approach and methods

2.1. Experimental means and facilities

This experimental study is carried out in the "Lucien Malavard" closed return-circuit wind tunnel at the University of Orléans, France. The model has a chord of 300 mm and is a rounded trailing-edge $NACA65_4 - 421$ circulation control-oriented airfoil (figure 2) with a curvature radius of 2% of the chord (6 mm). This airfoil is used on wind turbine blades at around 70% of the blade span and its shape is structurally interesting because its maximum thickness is located at around 50% of the chord length. Lift coefficient for different Reynolds numbers and angles of attack is shown in figure 3 as well as the comparison between the unmodified NACA airfoil and the $NACA65_4 - 421-CC$ one. The unmodified airfoil has been studied at the University of Orléans by Sicot et al. under static stall [12] and rotating stall [13] configurations. Lift coefficient is higher for the rounded trailing-edge configuration and it is proven in [14] that the roundness of the trailing-edge does not deteriorate the aerodynamic performance of the profile because its effect is compensated by the additional camber on the pressure side. The model has a 1.1 m wing span and it is studied in a 2D-flow configuration between two flat plates in the test section. The model is mounted on a 6-component floor balance that provides time averaged lift and drag forces. Mean pressure distribution around the airfoil is measured with twenty pressure taps implemented around the model between the leading-edge and 70% of the chord length and in the middle plane of the blade.

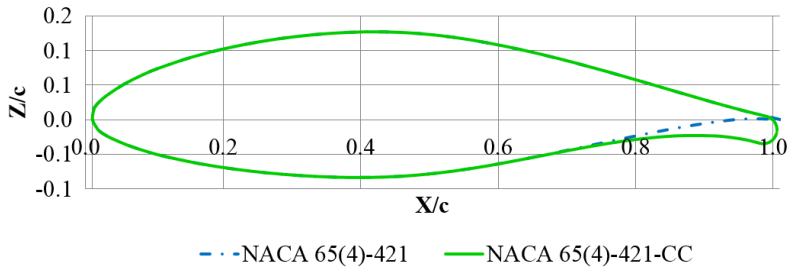

Figure 2. Original $NACA65_4 - 421$ airfoil (dotted line) and circulation control airfoil $NACA65_4 - 421{-}CC$(solid line)

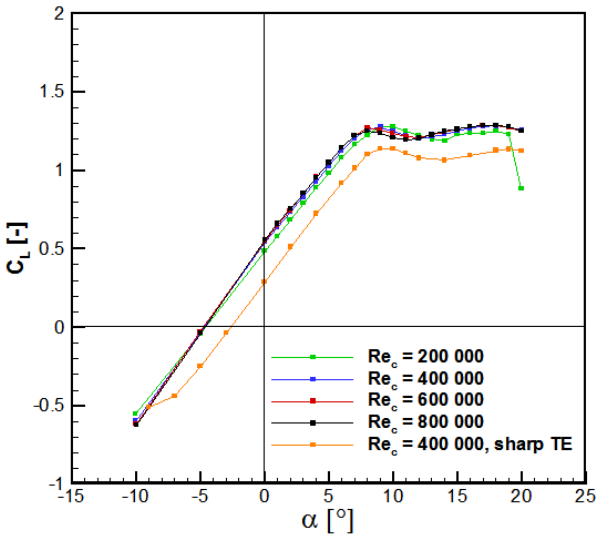

Figure 3. Lift coefficient versus angle of attack for different Reynolds numbers ($NACA65_4 - 421{-}CC$, except last curve $NACA65_4 - 421$) ([14])

Mean velocity fields around the trailing-edge are obtained via PIV (Particle Image Velocimetry) measurements made in the symmetry plane of the airfoil model. The PIV system consists, in the case of the wind-tunnel experiments discussed in section 4, of a Nd:Yag laser (2×200 mJ) emitting pulses with a 2.5 Hz emission rate. The light sheet is oriented in order to visualize simultaneously both pressure and suction sides of the airfoil. Seeding particles are micro-sized olive oil droplets sprayed by a PIVTEC seeding system and the particle diameter is of approximately $1\,\mu$ m. Images were acquired with a LaVision Imager LX camera (4032 px $\times$ 2688 px) and a 200 mm lens. The final resolution is of one vector every 0.4 mm with a 16 px $\times$ 16 px interrogation window with an overlap of 50%. One thousand image pairs are recorded. For the quiescent air experiments discussed in section 3, the same seeding system is used as well as a similar laser. The camera used is a TSI Power View (2048 px $\times$ 2048 px) with a 200 mm lens. This system allows a final resolution of one vector every 0.5 mm with a 32 px $\times$ 32 px interrogation window. Six hundred image pairs are recorded for every configuration. Due to laser reflections and plasma light emission, the first vector taken into account is 1 mm far from the model wall.

2.2. Plasma actuators

Dielectric Barrier Discharge (DBD) actuators consist of two copper electrodes that are positioned on both sides of a dielectric material as shown in figure 4 for a single DBD actuator. With the high voltage application, the ambient air is ionised and accelerated along the grounded electrode, creating an ionic wind that permits the manipulation of the flow in the near wall zone. This ionic wind diffuses along the wall in a similar way as a wall jet and has a maximum velocity of around 5 m/s for the actuators used in this project.

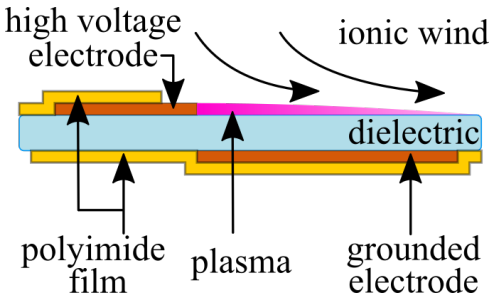

Figure 4. Scheme of the working principle of a single DBD plasma actuator

In this study, multi-DBD plasma actuators are implemented at the rounded trailing-edge of the model on both sides of a 3 mm thick PMMA cap. In this case, the multi-DBD actuators consists of the concatenation of two single DBD actuators. Figure 5 shows the geometry and the positioning of the electrodes for the whole set of actuators studied: actuators 1 and 2 (ACT1 and ACT2) are meant to increase the lift coefficient (C_l) while actuator 3 (ACT3) is meant to decrease the C_l. The span length of the electrodes is between 800 mm and 900 mm. The high voltage electrodes (or active electrodes) are serrated and powered with a laboratory-made AC-power supply up to 20 kV while the grounded one is linear and is encapsulated with the dielectric material of the model itself. The typical power consumption of every actuator is of around 40 W/m for the highest implemented voltage. All the distances between the electrodes remain the same for the three tested actuators and what does change is the positioning of these electrodes around the trailing-edge. While the actuator ACT1 is centered on the middle line of the trailing-edge curvature, the actuator ACT2 is shifted of an angle of 45º towards the pressure side of the airfoil with respect to this middle line. On the other hand, actuator ACT3 is shifted of an angle of 45º as well, but towards the suction side this time. Figure 6 shows a picture of the experimental set-up mounted on the wind tunnel section.

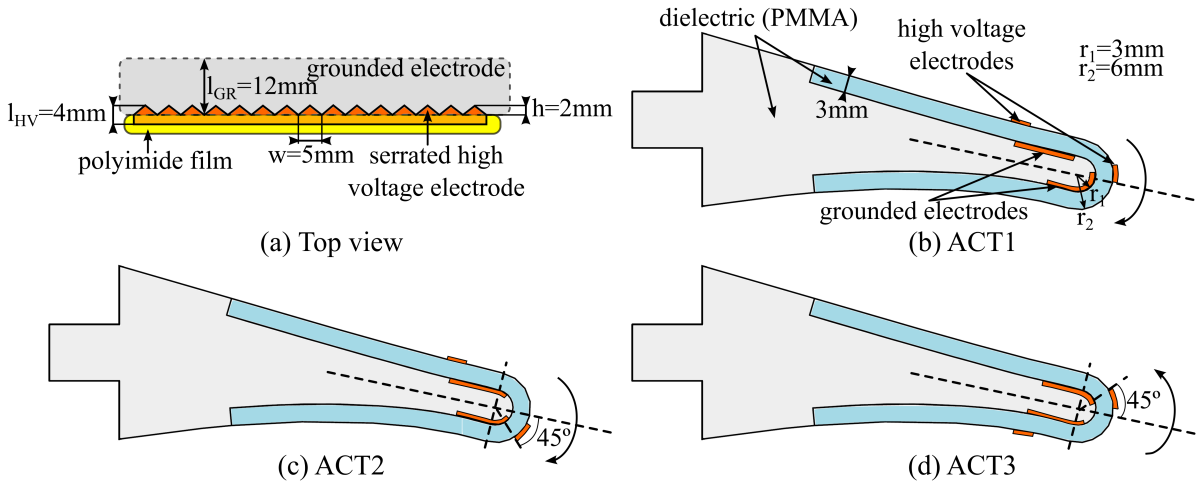

Figure 5. Configuration of the actuators: **(a)** top view of the electrodes geometry **(b)** positioning of the electrodes for the actuator 1 (ACT1, downward effect) **(c)** positioning of the electrodes for the actuator 2 (ACT2, downward effect) **(d)** positioning of the electrodes for the actuator 3 (ACT3, upward effect)

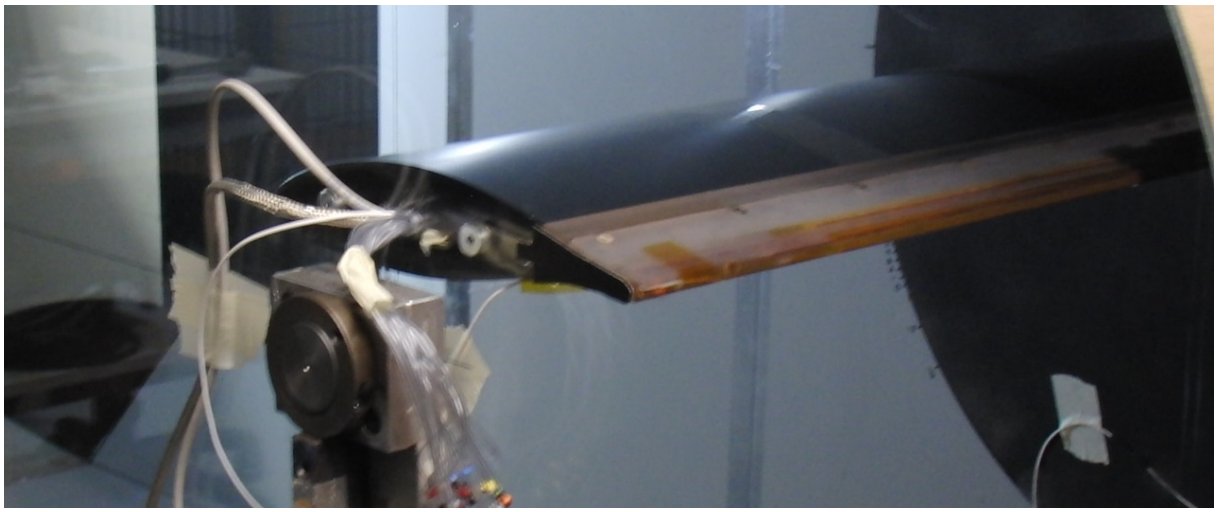

Figure 6. Photography of the airfoil model mounted on the wind tunnel test section

3. Jet topology under quiescent air conditions

PIV measurements were carried out under quiescent air conditions in order to characterize the topology of the ionic wind induced in the absence of an incoming flow in order to better understand the wake flow modification under actuation.

Figure 7 shows the time averaged magnitude velocity field of the flows induced by the actuators ACT1 and ACT2 under quiescent air conditions. The plotted vector profiles are obtained by interpolating the PIV measurement points along the normal lines to the model wall. On both flow fields two zones can be highlighted: one acceleration zone along the grounded electrodes where the ambient air is accelerated and the momentum transfer between the charged

particles takes place; and one diffusion zone, after the trailing-edge curvature where the induced jet diffuses along the model wall. The maximum ionic wind velocity is of around 4 m/s for both actuators. To evaluate the momentum transfer to the fluid the momentum coefficient is usually employed and defined as follows (equation 1):

$$C_\mu = \frac{\int_0^\infty \rho u(y)^2 \mathrm{d}y}{\frac{1}{2}\rho_\infty U_\infty^2 c} \tag{1}$$

Where ρ is the density, u is the longitudinal velocity, y is the normal direction to the model wall, ρ_∞ and U_∞ are the incoming flow density and velocity respectively and c is the chord of the airfoil. These actuators were characterized in a plane configuration in [15] and the obtained C_μ is of around 0.004 for a freestream velocity U_∞ of 10m/s (Re = 200000). As the plasma jet induces a small velocity (maximum jet speed of 5m/s), the momentum coefficient is low compared to other techniques such as continuous jets which C_μ is of around 0.02. However, the momentum coefficient is of the same order of magnitude as the one that can be obtained with synthetic jets (C_μ equal to 0.005) as can be found in [16]. Within the SMARTEOLE project, a comparison between plasma and fluidic jet actuators dedicated to circulation control around wind turbine airfoils is done ([17]) and an energy balance will be carried out once both control strategies are validated.

However, the jet topology is different for the actuators ACT1 and ACT2. While the actuator ACT1 ionic wind does not follow the model curvature perfectly, the actuator ACT2 does the 180º turn by following continuously the wall. Its jet is consequently thinner and shows a smaller diffusion. These results were expected as the electrodes of the actuator ACT2 are shifted of 45º towards the pressure side with respect to the ones of the actuator ACT1. This shifted configuration permits a more efficient rounding of the trailing-edge as the plasma is created closer to the pressure side. It is important to remember that these PIV measurements are made in the plane of symmetry of the blade and that it is assumed that the jet actuation is homogeneous along the wingspan. However, this assumption has not been verified and the ionic wind of the actuator ACT2 might have areas with a different topology along the span with eventually higher thickness and diffusion.

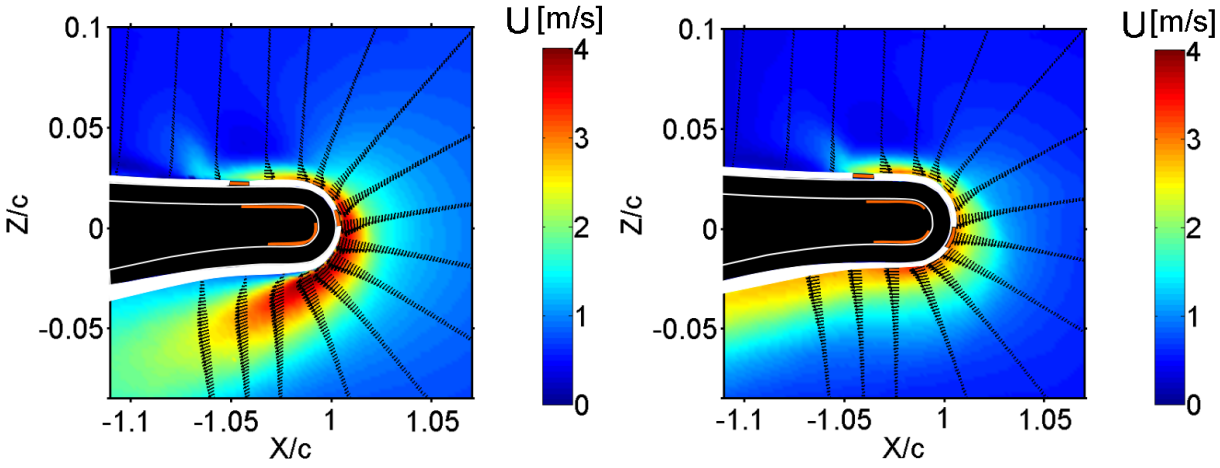

Figure 7. Time averaged magnitude velocity field and velocity vector profiles for **ACT1** (left) and **ACT2** (right) under quiescent air conditions ($V = 18kV$, $f = 1kHz$)

Figure 8 shows the time averaged magnitude velocity field of the flows induced by the actuators ACT2 and ACT3 under quiescent air conditions. The jet topology of the two actuators

is similar excepting that they blow in opposite directions. This is due to the fact that both actuators are shifted of an angle of 45^{o} towards the pressure and suction side respectively. As the model shape is roughly symmetrical on the pressure and suction sides, the ionic wind behaviour is comparable for both actuators. Because of the electrical nature of the surface plasma actuation, the tangential jet remains attached to the wall and follows its curvature in a different way than, for example, the fluidic jets that may benefit of the Coanda effect.

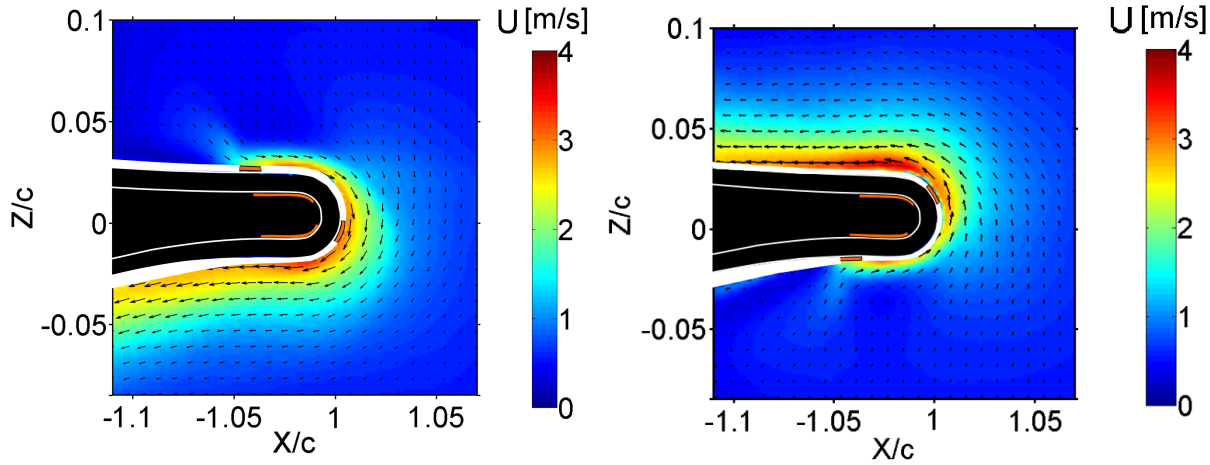

Figure 8. Time averaged magnitude velocity field and vector field for **ACT2** (left) and **ACT3** (right) under quiescent air conditions ($V = 18kV$, $f = 1kHz$)

4. Effect of the actuation on the flow

In this section are detailed the results of circulation control obtained with an incoming flow. First are shown the results concerning the modification of the aerodynamic loads and of the mean pressure around the airfoil under actuation. The effects of the circulation control on the wake topology will be then explained via the PIV results.

4.1. Effect of the flow control on the aerodynamic loads

Figure 9 shows the lift coefficient and lift to drag ratio as a function of the angle of attack for the baseline flow and the actuators ACT1 and ACT3 for an incoming flow velocity U_∞ of 10 m/s (Reynolds number equal to 200000). Every measurement point is the time average of a 20 s measurement of lift force at 1 kHz. By the effect of the actuation, the baseline C_l curve is translated towards higher lift coefficients for the actuator ACT1, and lower lift coefficients for the actuator ACT3. The maximum lift coefficient variation ΔC_l is of ± 0.08. This lift gain is equivalent to the one obtained by Kotsonis et al. [10] with a symmetrical airfoil and a Reynolds number of 140000. Because of the low momentum coefficient C_μ obtained with DBD actuators, this lift gain is small compared to the one that could be obtained with trailing-edge flaps or microtabs (yet microtabs are passive devices and the comparison between the two control strategies may be delicate). However, even if the lift coefficient gain is small, plasma actuators can serve as a proof of concept of active flow control. In addition to the assets mentioned in the introduction (no mobile parts, very quick time response, small weight), plasma actuators create a ionic wind that adheres to the wall without a Coanda effect and only by electrical effects.

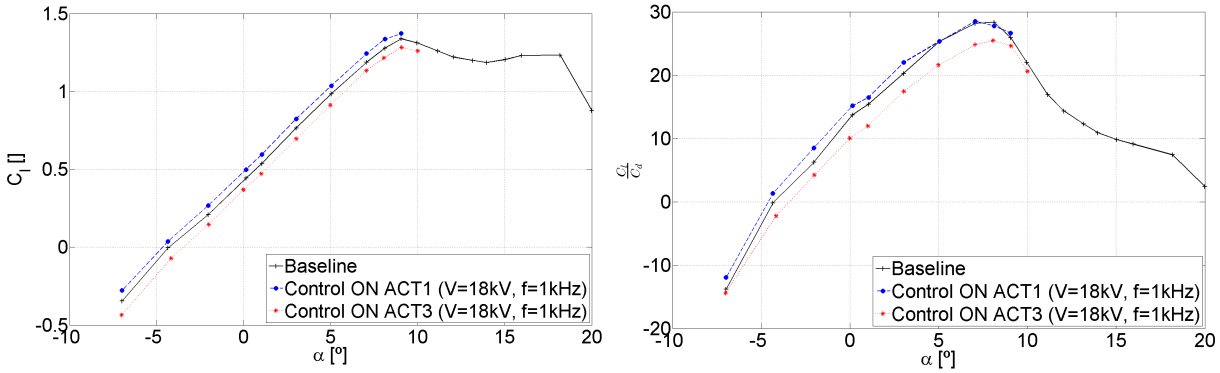

Figure 9. On the left, lift coefficient as a function of the angle of attack; on the right, lift to drag ratio as a function of the angle of attack ($U_\infty = 10m/s$ ($Re = 200000$))

Regarding the lift to drag ratio on figure 9, the baseline curve is also modified. The actuator ACT1 increases the lift to drag ratio for the angles of attack from $\alpha = -7$ to $\alpha = 5$ and for higher angles of attack the modified curve is superimposed to the baseline. The actuator ACT3 decreases the lift to drag ratio in a larger range of angles of attack and in a more pronounced way. Figure 10 shows the lift coefficient as a function of the applied voltage for $U_\infty = 10m/s$ and an angle of attack of $\alpha = 0°$. One can see that the higher the applied voltage, the higher the consequent lift coefficient will be.

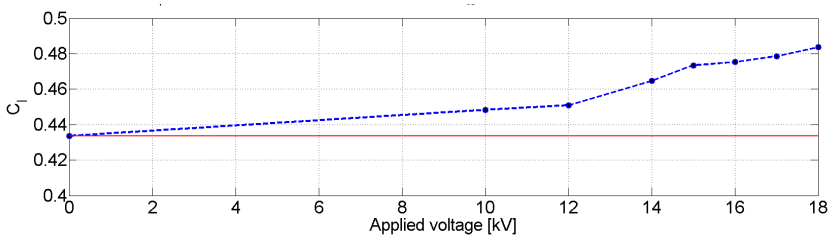

Figure 10. Lift coefficient as a function of the applied voltage (ACT1, $U_\infty = 10m/s$, $\alpha = 0°$)

Flow control effectiveness has also been highlighted by the mean pressure measurements carried out in the plane of symmetry of the airfoil. Figure 12 shows the pressure distribution around the airfoil for two angles of attack $\alpha = 0$ and $\alpha = 5$ and $U_\infty = 10m/s$. The absence of a suction peak at these low angles of attack is due to the nature of the airfoil which boundary layer remains laminar up to 50% of the chord. Figure 11 shows the pressure distribution over a $NACA65_4 - 421{-}CC$ airfoil without a removable trailing-edge and therefore with pressure taps located all around the airfoil. As the lift coefficient is the integration of the pressure coefficient C_p around the airfoil, the previously observed tendencies of the actuation can be confirmed for both angles of attack shown. For the actuator ACT1, which aims at increasing the lift coefficient the area between the curve is greater than the baseline one: the lift coefficient is hence increased. In the same way, the area inside the actuator ACT3 curve is smaller than the baseline one, the lift force in then decreased by the effect of the actuation. Usually, circulation control generates a low pressure area in the vicinity of the actuation. Because of the presence of the plasma actuators at the trailing-edge of the model, the pressure taps are only distributed up to 70% of the chord and these phenomena cannot be observed. Further analysis of the pitch moment measurements will be carried in order to better understand the pressure distribution at the trailing-edge with the actuation.

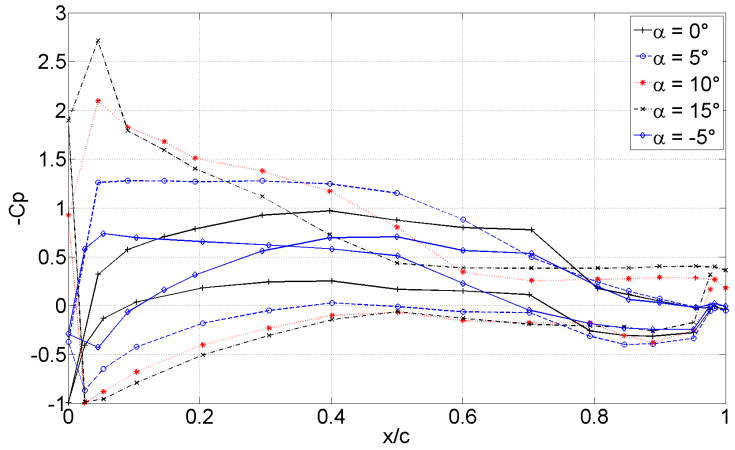

Figure 11. Pressure distribution over a NACA65$_4$ − 421−CC airfoil without a removable trailing-edge ($U_\infty = 10m/s$)

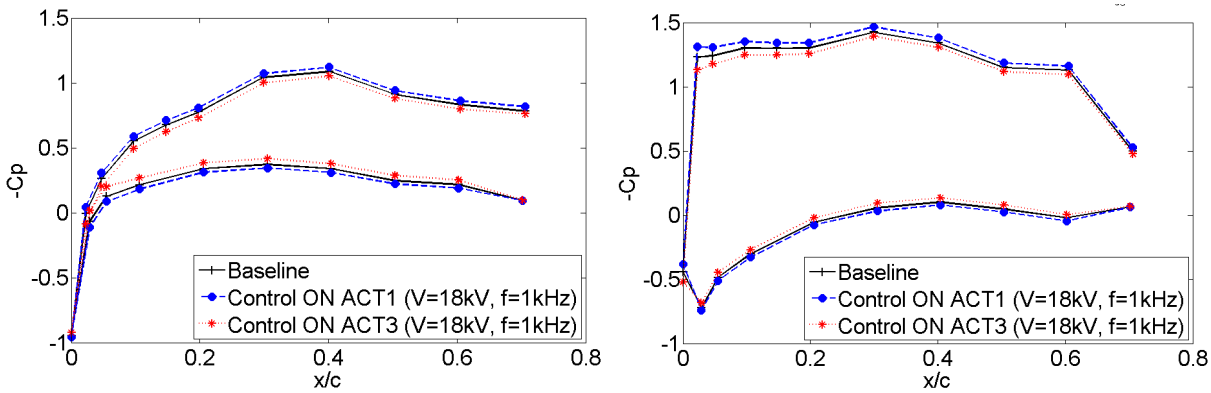

Figure 12. Pressure distribution around the airfoil at $\alpha = 0$ (left) and $\alpha = 5$ (right) and $U_\infty = 10m/s$

4.2. Effect of the circulation control on the flow topology

Figure 14 shows the non dimensional mean magnitude velocity field for the actuator ACT1 (without actuation) for $U_\infty = 10m/s$ and $\alpha = 0$. Because of the rounded trailing-edge, a small recirculation area appears in the wake of the airfoil showing two counter-rotating vortices characteristic of bluff bodies. If we consider an unsteady approach there is an alternate vortex shedding from the pressure and suction sides of the model that are related to a Von Karmann vortex street. This phenomena has been highlighted via hot wire measurements on the trailing-edge wake that show a characteristic Strouhal ($St = \frac{df}{U_\infty}$, where f is the frequency of the instability, d is the diameter of the trailing-edge roundness (d =12 mm) and U_∞ the incoming flow velocity) number of 0.17 (see figure 13). One can see that the actuation modifies the vortex shedding as this one seems to be more intense for the case under actuation and its frequency is slightly reduced. The rounded trailing-edge does not deteriorate the aerodynamic performance of the profile because the small drag penalty induced by the roundness is balanced by the additional camber as shown in [14].

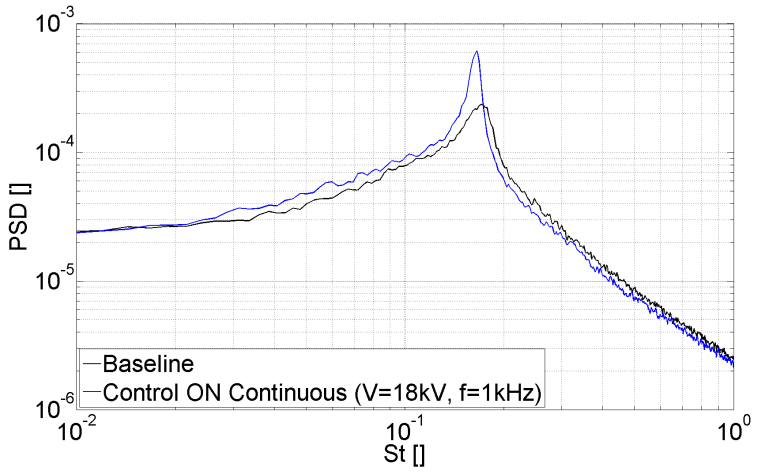

Figure 13. Power Spectral Density as a function of the Strouhal number for **ACT1** ($U_\infty = 10m/s$ and $\alpha = 0$)

Figure 15 shows the subtraction of the mean magnitude velocity field for the controlled flow and the baseline one for the actuator ACT1 for the previous angle of attack and incoming flow velocity. As under the effect of the actuation the recirculation area is deflected towards the pressure side, the lower zone of the wake shows a velocity deficit while the flow coming from the suction side is slightly faster in the controlled case than in the baseline one.

The actuation tends to deviate the wake towards the pressure or the suction side depending on the considered actuator. Figure 16 shows the velocity profiles on the wake 5% of the chord away from the trailing-edge for the actuators ACT1 and ACT3 ($U_\infty = 10m/s$ and $\alpha = 0$). As the actuator ACT1 blows from the suction side to the pressure side of the airfoil the wake is deflected towards the pressure side. On the contrary, the wake of the actuator ACT3 is deflected towards the suction side.

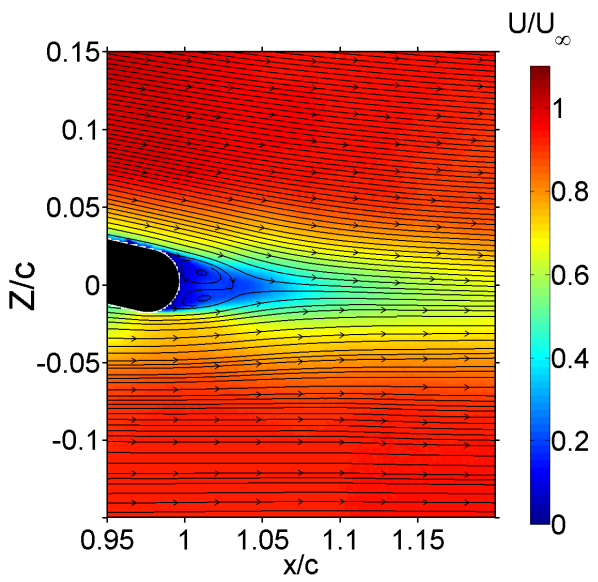

Figure 14. Non dimensional mean magnitude velocity field for **ACT1** without actuation at $\alpha = 0$ and $U_\infty = 10m/s$

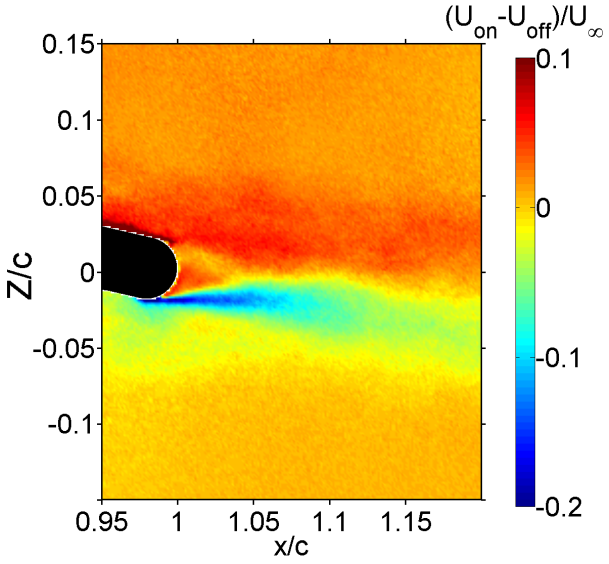

Figure 15. Subtraction of the mean magnitude velocity field for the controlled flow ($f = 1kHz$, $V = 18kV$) and the baseline one for the actuator **ACT1** at $\alpha = 0$ and $U_\infty = 10m/s$

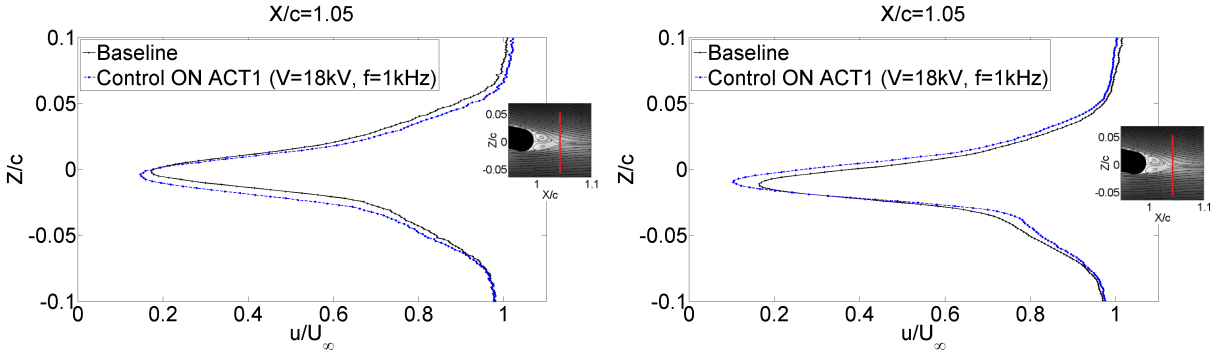

Figure 16. Velocity profiles with and without actuation ($f = 1kHz$, $V = 18kV$) for **ACT1** (left) and **ACT3** (right) at $\alpha = 0$ and $U_\infty = 10m/s$

5. Conclusion

To achieve the circulation control, three sets of multi DBD plasma actuators have been studied. The effectiveness of the control has been shown through load and pressure measurements: two actuators are able to increase the lift force and one to decrease it. PIV measurements permit the highlighting of the flow topology modification and the wake alteration by the effect of the actuation. A deeper analysis of the PIV results will be carried out order to examinate the flow alteration carefully.

Furthermore, a study is being carried on in order to design and implement an actuator that would be capable of increasing and decreasing the lift force by a particular positioning of the electrodes and without requiring the disassembly of the whole trailing-edge. Moreover, to better understand the transient aerodynamics and the unsteady response of the system, a dynamic analysis is carried out. The transient aerodynamics is being characterized by the synchronization of the pressure and balance acquisitions when the actuator is subjected to various high voltage

steps. The final goal of this characterization is the implementation of a closed loop active flow control.

Acknowledgements
This project is funded by the French national project SMARTEOLE (ANR-14-CE05-0034).

References

[1] Joslin R and Jones G 2006 *Applications of Circulation Control Technology* (AIAA)
[2] Kweder J, Panther C C and Smith J E 2008 *Int. J. Eng* **4** 411–429
[3] Johnson S, Case van Dam C P and Berg D E 2008 *SANDIA report 2008-4809*
[4] Benard N and Moreau E 2014 *Exp. in Fluids* **55** ISSN 0723-4864
[5] Walker S and Segawa T 2012 *Renewable Energy* **42** 105–110 ISSN 0960-1481
[6] Meijerink J and Hoeijmakers H 2011 Plasma actuators for active flow control on wind turbine blades *29th AIAA Applied Aerodynamics Conf.* June (Honolulu, Hawaii) pp 1–18
[7] Greenblatt D, Schulman M and Ben-Harav A 2012 *Renewable Energy* **37** 345–354 ISSN 0960-1481
[8] Jukes T N 2015 *Renewable Energy* **80** 644–654 ISSN 0960-1481
[9] Zhang P, Yan B, Liu a B and Wang J J 2010 *AIAA Journal* **48** 2213–2226
[10] Kotsonis M, Pul R and Veldhuis L 2014 *Exp. in Fluids* **55** ISSN 07234864
[11] Leroy A, Podlinski J, Devinant P and Aubrun S 2015 Circulation control by plasma actuators for load fluctuation alleviation *6th European Conference For Aeronautics and Space Sciences* (Krakow, Poland)
[12] Sicot C, Aubrun S, Loyer S and Devinant P 2006 *Experiments in Fluids* **41** 641–648 ISSN 07234864
[13] Sicot C, Devinant P, Loyer S and Hureau J *Journal of Wind Engineering and Industrial Aerodynamics* **96** 1320–1331
[14] Aubrun S, Leroy A and Devinant P 2015 Aerodynamic loads fluctuations alleviation by circulation control on wind turbine blades *50th AAAF International Conference on Applied Aerodynamics* (Toulouse, France)
[15] Leroy A, Podlinski J, Baleriola S, Devinant P and Aubrun S 2016 *Int. J. of Plasma Environmental Science and Technology (to be published)*
[16] McCormick D 2000 Boundary layer separation control with directed synthetic jets *AIAA 38th Aerospace Sciences Meeting and Exhibit* vol 2000-0519 (Reno, Nevada)
[17] Leroy A, Braud C, Baleriola S, Loyer S, Devinant P and Aubrun S 2016 Comparison of flow modification induced by plasma and fluidic jet actuators dedicated to circulation control around wind turbine airfoils (to be published) *TORQUE 2016 (to be published)*